Measurement of cosmic-ray carbon and oxygen energy spectra with CALET

Paolo Maestro *, for the CALET collaboration

Department of Physical Sciences, Earth and Environment, University of Siena, via Roma 56, 53100 Siena, Italy
INFN Sezione di Pisa, Polo Fibonacci, Largo B. Pontecorvo, 3, 56127 Pisa, Italy

Abstract

The CALorimetric Electron Telescope (CALET) is a space mission installed on the International Space Station (ISS) in August 2015. In addition to high precision measurements of the electron spectrum up to TeV scale, CALET will also investigate the mechanism of cosmic-ray (CR) acceleration and propagation in the Galaxy, by performing direct measurements of the energy spectra and elemental composition of CR nuclei from H to Fe, and the abundance of trans-iron elements up to about $Z = 40$. The instrument consists of two layers of segmented plastic scintillators to identify the particle charge, a thin (3 radiation lengths) tungsten-scintillating fiber calorimeter providing accurate particle tracking, and a thick (27 radiation lengths) calorimeter made of lead-tungstate crystal logs. In this paper, we discuss the analysis procedure developed to reconstruct and select carbon and oxygen nuclei in cosmic rays and present the preliminary measurement of their energy spectra based on the analysis of the data collected from October 2015 to February 2018.
© 2019 COSPAR. Published by Elsevier Ltd. All rights reserved.

1. Introduction

Direct measurements of charged cosmic rays (CR) providing information on their elemental composition and energy spectra up to the PeV energy scale are fundamental to achieve a better understanding of their origin, mechanism of acceleration at the astrophysical sources and propagation in the Galaxy. Recent observations of a spectral hardening in proton, helium (Aguilar et al., 2015; Adriani et al., 2011; Yoon et al., 2011; Yoon et al., 2017) as well as in heavy nuclei spectra (Ahn et al., 2010; Aguilar et al., 2017) around a few hundred GeV/n, compelled a revision of the standard paradigm of galactic CR based on diffusive shock acceleration in supernova remnants fol-

lowed by propagation in galactic magnetic fields, and prompted an intense theoretical activity to interpret these unexpected spectral features (Serpico, 2015; Tomassetti, 2012; Evoli et al., 2018; Ohira et al., 2016; Vladimirov et al., 2012; Ptuskin et al., 2013; Thoudam and Hörandel, 2014). In the meanwhile, new experimental efforts are being undertaken to accurately determine the onset of spectral hardening and extend its measurement up to the TeV scale (Atkin et al., 2017; Chang et al., 2017; Smith et al., 2017).

The CALorimetric Electron Telescope (CALET) is a space-based instrument optimized for the measurement of the all-electron spectrum (Adriani et al., 2017; Adriani et al., 2018), which can also measure, thanks to its wide dynamic range, large thickness, accurate tracking and charge identification capabilities, individual chemical elements in CR from proton to iron and above in the energy range up to ~1 PeV. In this paper, we describe the analysis procedure for C and O flux measurements and present their

* Address: Department of Physical Sciences, Earth and Environment, University of Siena, via Roma 56, 53100 Siena, Italy.
E-mail address: paolo.maestro@pi.infn.it.

preliminary energy spectra based on the data collected in 733 days of CALET operation onboard the International Space Station (ISS).

2. CALET instrument

The CALET instrument consists of three detectors: a CHarge Detector (CHD), a finely segmented pre-shower IMaging Calorimeter (IMC), and a Total AbSorption Calorimeter (TASC). CHD consists of a pair of plastic scintillator hodoscopes arranged in two orthogonal layers (CHDX, CHDY). It can resolve individual chemical elements from $Z = 1$ to $Z = 40$, with excellent charge resolution.

The IMC consists of 7 tungsten plates interleaved with double layers of $1\ mm^2$ cross-section scintillating fibers (SciFi), arranged in belts along orthogonal directions and readout by multianode photomultiplier tubes (PMTs), capped by an additional SciFi layer pair. Its fine granularity (448 SciFi per layer) allows us to accurately image the longitudinal and lateral profiles of the initial shower development, enhancing the electron-proton discrimination and providing electron-gamma separation. Moreover it provides accurate particle tracking and CR identification by multiple dE/dx sampling.

The TASC is a homogeneous calorimeter made of 192 Lead Tungstate (PWO) "logs" ($2 \times 1.9 \times 32\ cm^3$) arranged in 12 layers, with a total thickness equivalent to 27 radiation lengths (X_0). The logs in the top layer are readout by PMTs, while a dual photodiode/avalanche-photodiode system is used for the readout of the remaining layers. A dynamic range of more than six orders of magnitude, necessary to span an energy range from singly-charged minimum ionizing particles (*mip*) to 1 PeV showers, is covered by using front-end electronics with dual gain range for each channel. The TASC was designed to determine the energy of the incident electrons and gamma rays with an excellent energy resolution, better than 2% above 100 GeV, and provide a high discrimination between electromagnetic (e.m.) and hadronic cascades.

The total thickness of the CALET instrument is equivalent to 30 X_0 and 1.3 proton interaction lengths (λ_I). The geometrical factor is 0.12 m^2sr and the total weight is 613 kg.

Calibration and test of the instrument took place at CERN SPS during five campaigns between 2010 and 2015 with beams of electrons, protons and relativistic ions (Akaike, 2015; Bigongiari, 2015; Niita et al., 2015).

CALET was launched on August 19, 2015 by the Japanese rocket H-II Transfer Vehicle (HTV-5) and installed on the Japanese Experiment Module Exposure Facility of the ISS for a 5-year mission. The on-orbit commissioning phase aboard the ISS was successfully completed in the first days of October 2015, and since then the instrument has been taking science data continuously (Asaoka et al., 2018).

3. Data analysis

We have analyzed 733 days of flight data (FD) collected from October 13, 2015 to February 28, 2018. Energy calibration of each channel of CHD, IMC and TASC is performed by using penetrating proton and He particles, selected by a dedicated trigger mode. Raw signals are corrected for non-uniformity in light output, gain differences among the channels, time and temperature dependence (Asaoka et al., 2017; Niita et al., 2015). After calibration, each CR particle is reconstructed and each event assigned a charge and an energy. Carbon and oxygen events are then selected and sorted into energy intervals and the number of counts in each bin is corrected for several effects in order to compute the energy spectrum. The various steps of the analysis procedure are described in the following subsections.

Simulated data produced with a Monte Carlo (MC) program based on the FLUKA package (Ferrari et al., 2005; Böhlen et al., 2014) and employing the hadronic interaction model DPMJET-III (Roesler et al., 2000), are used in this analysis to validate and tune the reconstruction method and evaluate event reconstruction efficiencies, background contaminations and the energy response matrix. A detailed description of the detector configuration was implemented in the MC program, including individual modelization of the electronic noise and photostatistics fluctuations of each channel signal.

3.1. Preselection

Events detected by the onboard high-energy shower trigger (HET) are used in this analysis. HET is based on the coincidence of the signal of the top TASC layer (TASCX1) and the sum of signals of the last two layers of SciFi belts in each IMC view, with thresholds chosen to ensure full efficiency for electrons above 10 GeV. HET efficiency for C and O nuclei was directly measured using a subset of FD taken with the same trigger logic, but with a lower threshold that allows to detect penetrating particles. HET efficiency curves as a function of the TASC total energy deposit (Fig. 1) show a good agreement with predictions from MC simulations.

An offline trigger confirmation is applied to HE-triggered events, by requiring that the TASCX1 signal is larger than 2 GeV (equivalent to the energy release of 100 *mip*'s in a crystal log) and the summed signals of the last two pairs of IMC SciFi layers are larger than 50 *mip*'s signal.

Moreover, in order to remove possible events triggered by particles entering the TASC from lateral sides or with significant lateral leakage, the energy deposits in TASCX1 and in the lateral TASC crystals (separately in each detector view) are required to be lower than 40% of the total energy deposit in TASC.
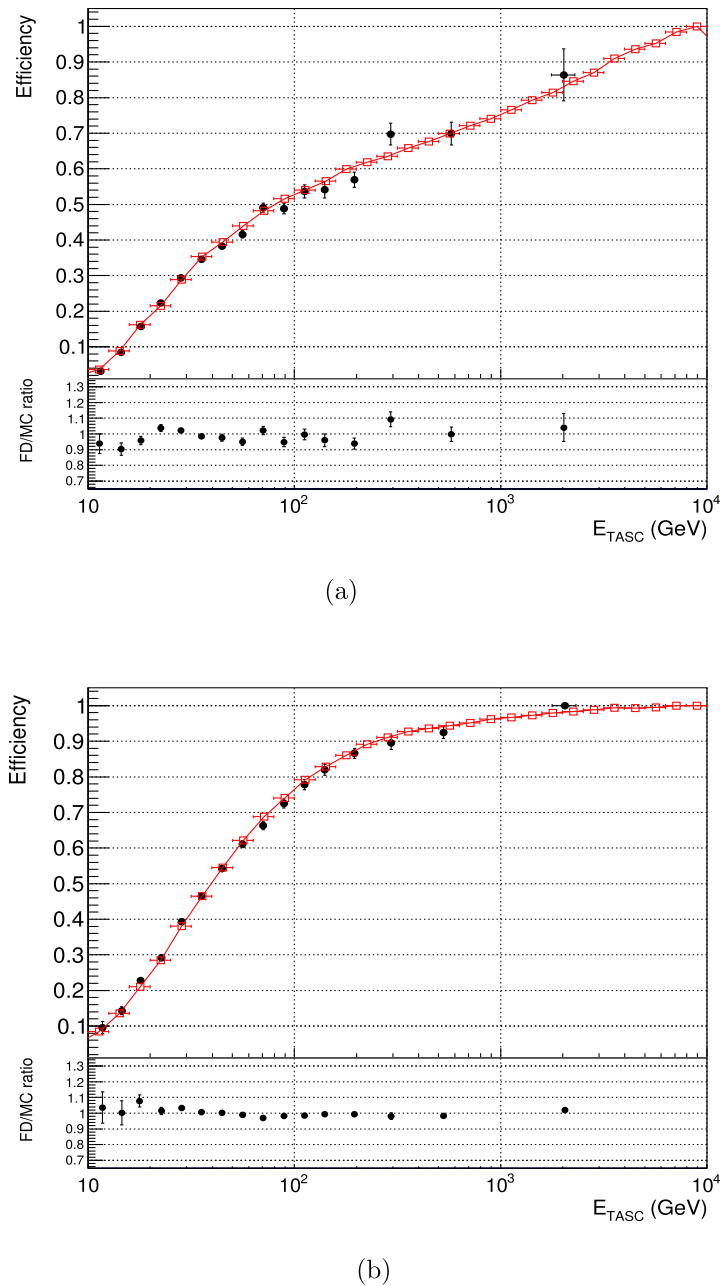
Fig. 1. HET efficiency as a function of the deposited energy in TASC for C (a) and O (b) nuclei as derived from FD (black dots) and MC (red rectangles). The FD to MC efficiency ratio is shown in the small canvas. (For interpretation of the references to colour in this figure legend, the reader is referred to the web version of this article.)

3.2. Track reconstruction

An original reconstruction method of the primary particle direction based on a combinatorial Kalman filter (KF) algorithm (Strandlie and Frühwirth, 2010; Frühwirth, 1987) was developed. This method exploits the fine granularity and imaging capability of the IMC and provides robust track finding and fitting, allowing to identify the incident CR track in a large amount of shower particle tracks backscattered from TASC. Track finding problem is decomposed in two independent two-dimensional problems in the XZ and YZ views, respectively, since IMC SciFi layers are oriented only in either x or y direction, and placed at a different z coordinates (Fig. 2). Neighbours hits (i.e. SciFi with signal >0.5 *mip*) in each IMC layer are clustered, and the cluster positions are taken as candidate track points for the combinatorial KF. A candidate track is created for each possible combination of clusters in the two upper layers in each view. Each track is fitted to a straight line and its predicted intercept on the next layer is used to associate a new cluster to the track. The procedure is iterated up to the last layer, unless the fit gives a large χ^2 value (>10) or more than two points are missing along the track; in this case the track is discarded. Among all the candidate
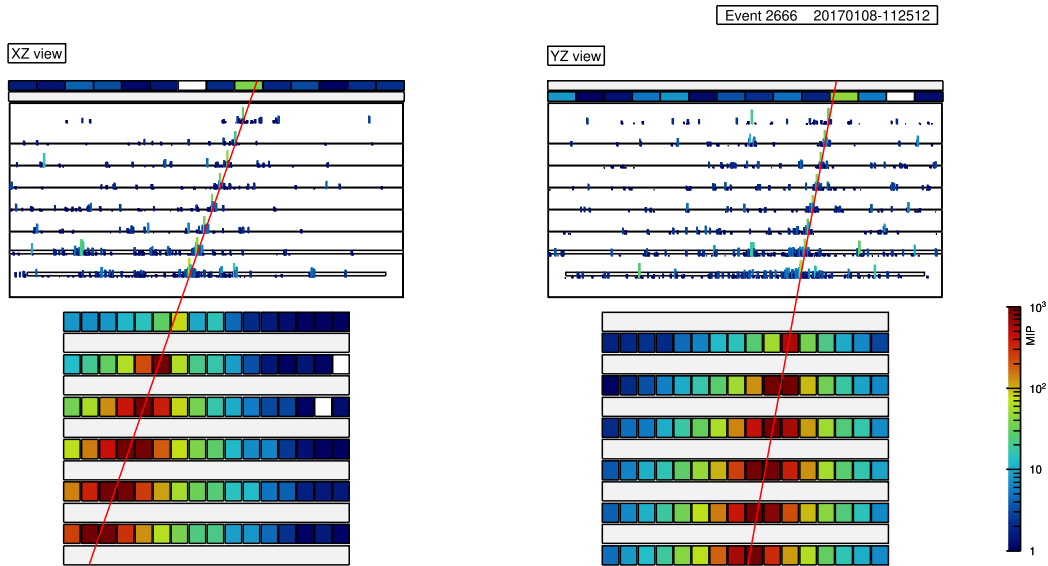
Fig. 2. Image of an exemplary carbon event with a shower energy in TASC of ∼11 TeV. The straight (red) lines represent the projections of the reconstructed particle trajectory in the XZ and YZ views, respectively. The logarithmic color scale represents the signal amplitude (expressed in units of *mip*) detected in each CHD, IMC and TASC channel. (For interpretation of the references to colour in this figure legend, the reader is referred to the web version of this article.)

tracks reconstructed by the combinatorial KF algorithm, the one with the largest energy deposited in the associated clusters and passing closest to the shower core in TASC, is chosen as the primary particle track.

The track fitting algorithm has been extensively validated with simulated data and good agreement was found between MC and FD distributions of reconstructed incident angle and impact point coordinates on top of CHD (Maestro and Mori, 2017). An angular resolution of ∼ 0.1° is found for C and O nuclei. The resolution of the impact point on CHD is ∼220 μm.

Events with a well-fitted primary track crossing the detector from CHD top to TASC bottom, with 2 cm margins at TASCX1, are used in this analysis. Additional cuts on χ^2/ndf (< 10) of the track fit and the number of track points (> 4) in each view are applied to ensure good track quality.

3.3. Charge identification

The identification of the charge Z of a CR particle is based on independent samplings of its specific ionization dE/dx measured with CHD and IMC. The particle trajectory is used to locate the CHD paddles and IMC SciFi traversed by the primary particle and determine the path length correction (proportional to sec θ, θ being the angle between the particle trajectory and the z-axis of the instrument) to be applied to the signals. For IMC, the sum of the signals of the crossed SciFi in each layer and its two neighbours is used. Three independent dE/dx measurements are obtained, one for each CHD layer and one by averaging the specific ionization yields in the first eight IMC layers. In order to suppress the contribution of possible signals of secondary tracks wrongly associated to the track of

the primary nucleus, only dE/dx signals larger than 1.5 MeV/mm (corresponding to the energy released in a SciFi by 10 *mip*'s) are used in the mean calculation.

The mean specific ionization yields derived from FD for each nuclear species can be fitted to a function of nominal Z^2, which, according to the "halo" model (Marrocchesi et al., 2011), parametrises dE/dx as the sum of two contributions ("core" and "halo", respectively)

$$\frac{dE}{dx} = \frac{A(1-f_h)\alpha Z^2}{1 + B_S(1-f_h)\alpha Z^2 + C_S\alpha^2 Z^4} + Af_h\alpha Z^2 \quad (1)$$

where the parameter f_h represents the fraction of energy deposited in the halo; B_S and C_S are parameters related to the strength of the scintillation quenching effects; A is an overall normalization constant; α is close to 2 MeV g^{-1} cm^2 for a plastic scintillator.

The parameters are extracted from the fits separately for CHDX, CHDY (Fig. 3) and IMC. These three calibration curves are then used to reconstruct three charge values (Z_{CHDX}, Z_{CHDY}, Z_{IMC}) from the measured dE/dx yields on an event-by-event basis.

The resulting distribution of the reconstructed charge combining Z_{CHDX} and Z_{CHDY} is shown in Fig. 4. An excellent charge resolution $\sigma_Z \sim 0.15e$ (charge unit) and $\sim 0.24e$ is estimated for CHD and IMC, respectively, in the elemental range from Be to O.

In this analysis, C and O nuclei are selected by applying, separately to Z_{CHDX}, Z_{CHDY} and Z_{IMC}, a $\pm 2\sigma_Z$ cut around the mean charge value. Particles that suffered a charge-changing nuclear interaction in the upper part of the instrument are removed by the three combined charged selections and by requiring the consistency, within 30%, between the mean values of dE/dx measurements in the first 4 IMC layers in each detector view.
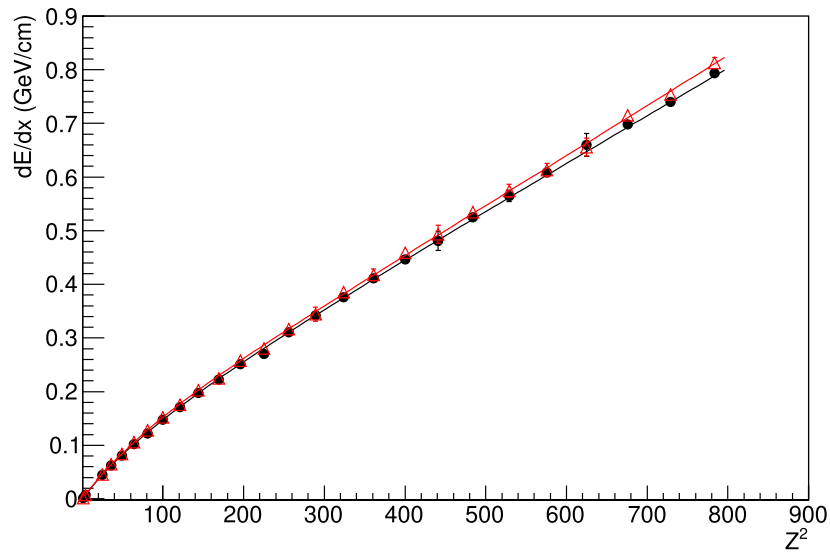
Fig. 3. Mean value of dE/dx for CHDX (black dots) and CHDY (triangles) as a function of nominal Z^2 of each nuclear species from Be to Fe in cosmic rays. The lines represent "halo" model functions (Eq. (1)) fitted to the data.
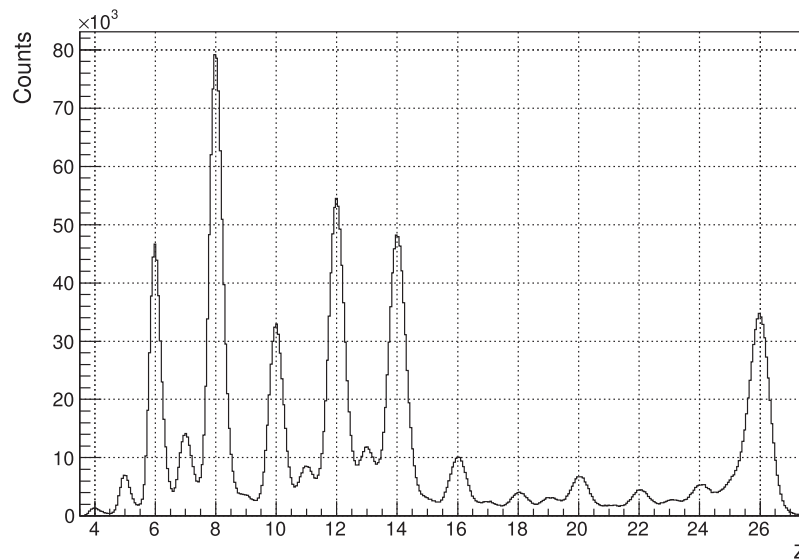

Fig. 4. Charge distribution in the elemental range from Be to Fe, as measured by the combined CHD layers using a subset of FD.

3.4. Energy measurement

The shower energy of each event is calculated as the sum of the calibrated energy deposits (E_{TASC}) of all the TASC channels. Distributions of E_{TASC} for C and O candidate events selected in this analysis are shown in Fig. 5, together with the background expected from other nuclei mis-identified as C or O. Contamination of each nuclear species with $Z > 4$ is estimated by rescaling its E_{TASC} distribution in FD by the ratio, estimated from MC, of its reconstruction efficiency to the probability that it is mis-identified for C or O. Background due to proton and helium is computed by normalizing their E_{TASC} distributions from MC to the number of events expected from previous flux measurements. It turned out that the total background in the selected C and

O event samples is negligible: $< 1\%$ up to $E_{TASC} \sim 5 \times 10^3$ GeV, and $\sim 2\%$ above.

Unlike for electrons, the energy released in TASC by interacting CR nuclei is only a fraction of the primary particle energy with large event-to-event fluctuations due to the significant hadronic shower leakage out of TASC. For C and O nuclei, the deposited energy in TASC corresponds to 20–30% of the primary energy, because of the incomplete longitudinal containment of the hadronic showers in a 1.3 λ_I thich calorimeter; the energy resolution is $\sim 30\%$, nearly independent of energy. For flux measurement, energy unfolding is necessary to correct the E_{TASC} distributions of selected C and O candidates for significant bin-to-bin migration effects, due to the limited energy resolution. In this analysis, we apply the iterative unfolding
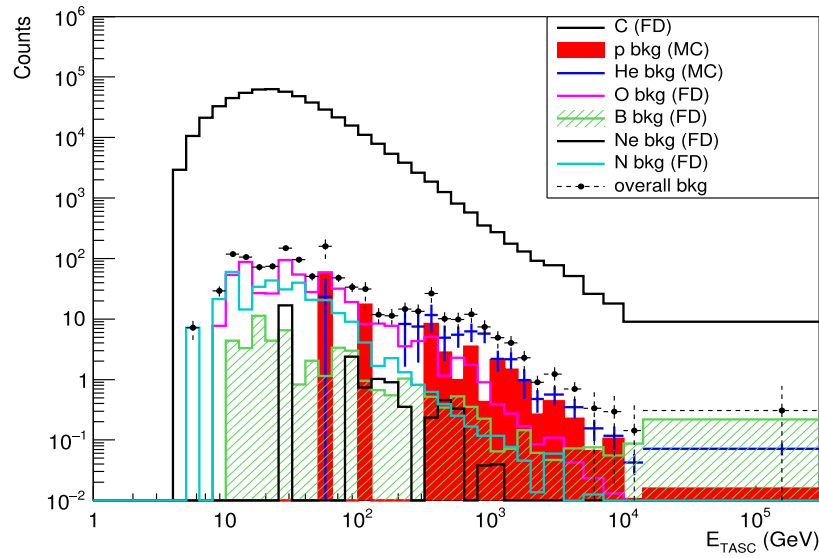
(a)
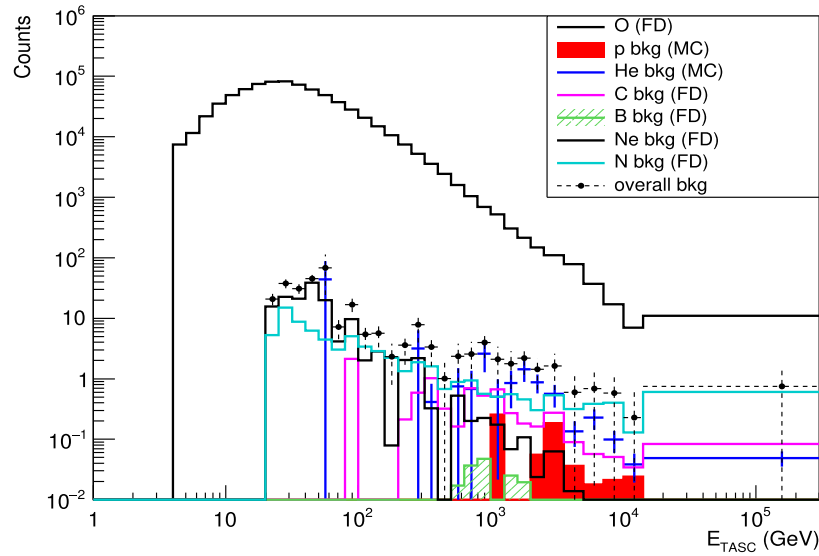
(b)

Fig. 5. Distribution of the total energy deposited in TASC by the selected C (*a*) and O (*b*) nuclei in FD (black line) and contamination from different nuclei. Overall background is represented by the black dots.

method based on the Bayes' theorem (D'Agostini, 1995) implemented in the RooUnfold package (Adye, 2011) in the ROOT analysis framework (Brun and Rademarkers, 1997). The response matrix, each element of which represents the probability that primary nuclei in a certain energy interval of the CR spectrum produce an energy deposit in a given bin of E_{TASC}, is derived using MC simulation after applying the same selection procedure as for FD (Fig. 6).

3.5. Energy spectrum

The energy spectrum is calculated as

$$\Phi\left(\widehat{E}\right) = \frac{N(E)}{\Delta E \times \varepsilon(E) \times S\Omega \times T} \quad (2)$$

$$N(E) = U\left(N_{obs}(E_{TASC}) - N_{bg}(E_{TASC})\right) \quad (3)$$

where $\widehat{E}$ is the median kinetic energy of the $[E, E + \Delta E]$ bin, ΔE the energy bin width, $\varepsilon(E)$ the overall selection efficiency, T is the exposure time, $S\Omega$ the "fiducial" geometrical acceptance, $N(E)$ the bin content in the unfolded distribution, $U()$ is the unfolding procedure based on Bayes' theorem, $N_{obs}(E_{TASC})$ the bin content of observed energy distribution (including background), $N_{bg}(E_{TASC})$
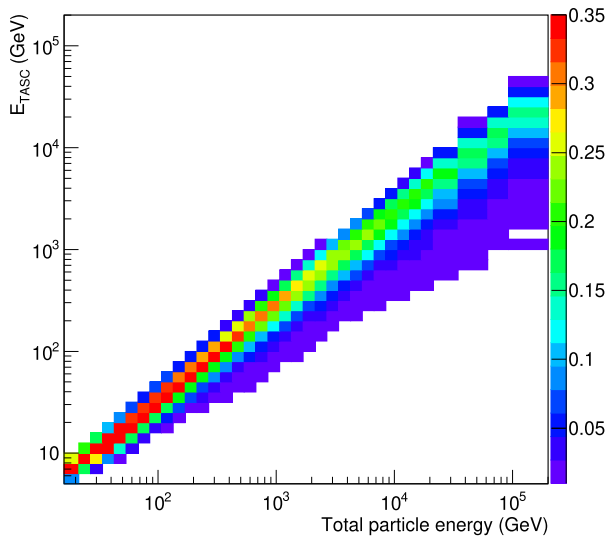
Fig. 6. Response matrix for oxygen derived from MC simulations by applying the same selection procedure as for FD. The color scale is associated to the probability that nuclei of a given energy produce showers in different intervals of E_{TASC}. (For interpretation of the references to colour in this figure legend, the reader is referred to the web version of this article.)

the bin content of background events in observed energy distribution.

4. Preliminary results

The preliminary energy spectra of CR carbon and oxygen nuclei measured with CALET in 733 days of operation are shown in Fig. 7. The measurements cover an interval of kinetic energy per particle from ~150 to ~10^5 GeV. Error bars of CALET data represent the statistical uncertainty only. The CALET preliminary results are compared with previous observations from space-based (HEAO-3-C2 (Engelmann et al., 1990), CRN (Müller et al., 1991), PAMELA (Adriani et al., 2014), AMS (Aguilar et al., 2017)) and balloon-borne (balloons flown in the '70 from Palestine (Texas) (Simon et al., 1980), ATIC-2 (Panov et al., 2009), TRACER (Ave et al., 2008), CREAM-II (Ahn et al., 2009)) experiments.

5. Summary

The preliminary results of carbon and oxygen spectra demonstrate the excellent capability of CALET to measure heavy nuclei in CR with high statistics, excellent charge separation and over a wide energy range. Further
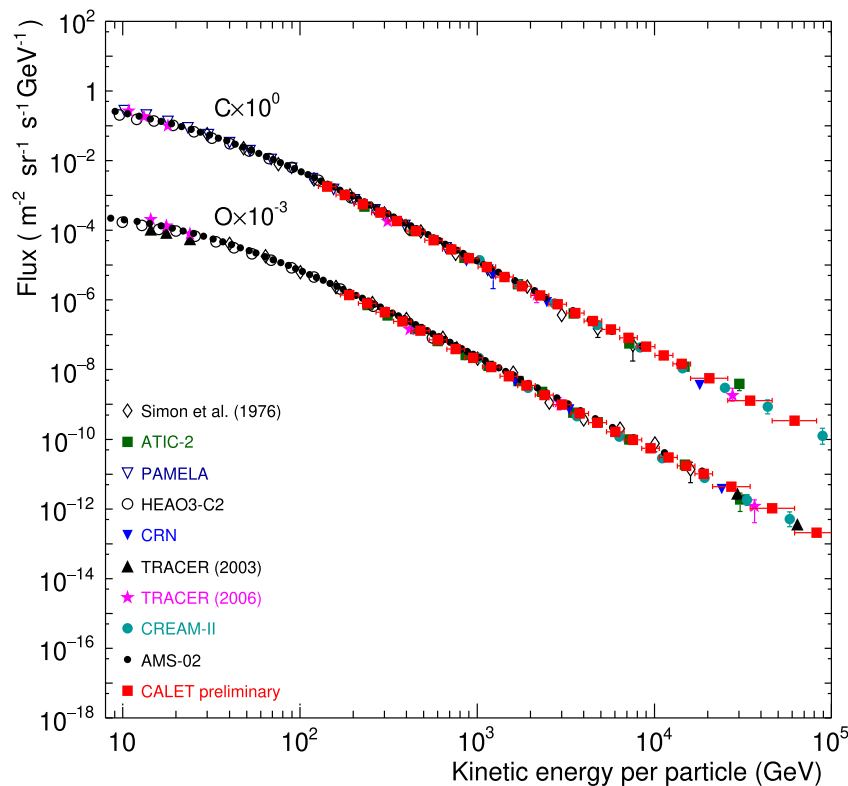

Fig. 7. Preliminary fluxes of CR carbon and oxygen nuclei measured with CALET (red markers) as a function of kinetic energy per particle, compared with previous direct observations (Simon et al., 1980; Engelmann et al., 1990; Müller et al., 1991; Panov et al., 2009; Ave et al., 2008; Obermeier et al., 2011; Aguilar et al., 2017; Adriani et al., 2014; Ahn et al., 2009). Error bars of CALET data represent the statistical uncertainty only. (For interpretation of the references to colour in this figure legend, the reader is referred to the web version of this article.)

analysis using an increased data set and including a detailed assessment of systematic uncertainties, is ongoing, aimed at investigating possible spectral features in the CR spectra.

References

Adriani, O., Barbarino, G.C., Bazilevskaya, G.A., et al., 2011. PAMELA measurements of cosmic-ray proton and helium spectra. Science 332, 69–72.

Adriani, O., Barbarino, G.C., Bazilevskaya, G.A., et al., 2014. Measurement of boron and carbon fluxes in cosmic rays with the PAMELA experiment. Astrophys. J. 791, 93, 11pp.

Adriani, O., Akaike, Y., Asano, K., et al., 2017. Energy spectrum of cosmic-ray electron and positron from 10 GeV to 3 TeV observed with the Calorimetric Electron Telescope on the International Space Station. Phys. Rev. Lett. 119, 181101, 6pp.

Adriani, O., Akaike, Y., Asano, K., et al., 2018. Extended measurement of the cosmic-ray electron and positron spectrum from 11 GeV to 4.8 TeV with the calorimetric electron telescope on the international space station. Phys. Rev. Lett. 120, 261102, 7pp.

Adye, T., 2011. Unfolding algorithms and tests using RooUnfold, arXiv:1105.1160v1.

Aguilar, M., Aisa, D., Alpat, B., et al., 2015. Precision measurement of the proton flux in primary cosmic rays from rigidity 1 GV to 1.8 TV with the alpha magnetic spectrometer on the international space station. Phys. Rev. Lett. 114, 171103, 9pp.

Aguilar, M., Ali Cavasonza, L., Alpat, B., et al., 2017. Observation of the identical rigidity dependence of He, C, and O cosmic rays at high rigidities by the alpha magnetic spectrometer on the International Space Station. Phys. Rev. Lett. 119, 251101, 8pp.

Ahn, H.S., Allison, P., Bagliesi, M.G., et al., 2009. Energy spectra of cosmic-ray nuclei at high energies. Astrophys. J. 707, 593–603.

Ahn, H.S., Allison, P., Bagliesi, M.G., et al., 2010. Discrepant hardening observed in cosmic-ray elemental spectra. Astrophys. J. Lett. 714, L89–L93.

Akaike, Y. (CALET collaboration) 2015. Simulations for CALET Energy Calibration Confirmed Using CERN-SPS Beam Tests. In: Proceedings of Science (ICRC2015), 613.

Asaoka, Y., Akaike, Y., Komiya, Y., et al., 2017. Energy calibration of CALET onboard the International Space Station. Astropart. Phys. 91, 1–10.

Asaoka, Y., Ozawa, S., Torii, S., et al., 2018. On-orbit operations and offline data processing of CALET onboard the ISS. Astropart. Phys. 100, 29–37.

Atkin, E., Bulatov, V., Dorokhov, V., et al., 2017. First results of the cosmic ray NUCLEON experiment. JCAP 07, 020.

Ave, M., Boyle, P.J., Gahbauer, F., et al., 2008. Composition of primary cosmic-ray nuclei at high energies. Astrophys. J. 678, 262–273.

Bigongiari, G. (CALET collaboration), 2015. CALET perspectives for calorimetric measurements of high energy electrons based on beam test results. In: Proceedings of Science (ICRC2015), 592.

Böhlen, T.T., Cerutti, F., Chin, M.P.W., et al., 2014. The FLUKA Code: developments and challenges for high energy and medical applications. Nucl. Data Sheets 120, 211–214.

Brun, R., Rademarkers, F., 1997. ROOT: an object oriented data analysis framework. Nucl. Instr. Meth. A 389, 81–86.

Chang, J., Ambrosi, G., An, Q., et al., 2017. The DArk matter particle explorer mission. Astropart. Phys. 95, 6–24.

D'Agostini, G., 1995. A multidimensional unfolding method based on Bayes' theorem. Nucl. Instr. Meth. A 362, 487–498.

Engelmann, J.J., Ferrando, P., Soutoul, A., et al., 1990. Charge composition and energy spectra of cosmic-ray nuclei for elements from Be to NI – results from HEAO-3-C2. Astron. Astrophys. 233, 96–111.

Evoli, C., Blasi, P., Morlino, P.G., Aloisio, R., 2018. Origin of the cosmic ray galactic halo driven by advected turbulence and self-generated waves. Phys. Rev. Lett. 121, 021102, 5pp.

Ferrari, A., Sala, P.R., Fassó, A., Ranft, J., 2005. FLUKA: a multi-particle transport code. CERN-2005-10, INFNTC_0511, SLAC-R-773.

Frühwirth, R., 1987. Application of Kalman filtering to track and vertex fitting. Nucl. Instr. Meth. A 262, 444–450.

Maestro, P. Mori, N. (CALET collaboration), 2017. Particle tracking in the CALET experiment. In: Proceedings of Science (ICRC2017), 208.

Marrocchesi, P.S., Adriani, O., Akaike, A., et al., 2011. Beam test performance of a scintillator-based detector for the charge identification of relativistic ions. Nucl. Instr. Meth. A 659, 477–483.

Müller, D., Swordy, S.P., Meyer, P., et al., 1991. Energy spectra and composition of primary cosmic rays. Astrophys. J. 374, 356–365.

Niita, T., Torii, S., Akaike, Y., et al. CALET collaboration, 2015. Energy calibration of Calorimetric Electron Telescope (CALET) in space. Adv. Space Res. 55, 2500–2508.

Obermeier, A., Ave, M., Boyle, P., et al., 2011. Energy spectra of primary and secondary cosmic-ray nuclei measured with TRACER. Astrophys. J. 742, 14, (11 pp).

Ohira, Y., Kawanaka, N., Ioka, K., 2016. Cosmic-ray hardenings in light of AMS-02 data. Phys. Rev. D 93, 083001, 7pp.

Panov, A.D., Adams, J.H., Ahn, H.S., et al., 2009. Energy spectra of abundant nuclei of primary cosmic rays from the data of ATIC-2 experiment: final results. Bull. Russ. Acad. Sci. 73, 564–567.

Ptuskin, V., Zirakashvili, V., Seo, E.S., 2013. Spectra of cosmic-ray protons and helium, produced in supernova remnants. Astrophys. J. 763, 47, 5pp.

Roesler, S., Engel, R., Ranft, J., 2000. The Monte Carlo Event Generator DPMJET-III. In: Proceedings of the Monte Carlo Conference, Lisbon, pp. 1033–1038.

Serpico, P., 2015. Possible physics scenarios behind cosmic-ray anomalies. In: Proceedings of Science (ICRC2015), 009.

Simon, M., Spiegelhauer, H., Schmidt, W.S.K., et al., 1980. Energy spectra of cosmic-ray nuclei to above 100 GeV per nucleon. Astrophys. J. 239, 712–724.

Smith, J., Amare, Y., Anderson, T., et al., 2017. The Cosmic Ray Energetics And Mass for the International Space Station (ISS-CREAM) Instrument. In: Proceedings of Science (ICRC2017), 199.

Strandlie, A., Frühwirth, R., 2010. Track and vertex reconstruction: from classical to adaptive methods. Rev. Mod. Phys. 82, 1419–1458.

Thoudam, S., Hörandel, J.R., 2014. GeV-TeV cosmic-ray spectral anomaly as due to reacceleration by weak shocks in the Galaxy. Astron. Astrophys. 567, A33, 10pp.

Tomassetti, N., 2012. Origin of the cosmic-ray spectral hardening. Astrophys. J. Lett. 752, L13, 5pp.

Vladimirov, A., Johannesson, G., Moskalenko, I., Porter, T., 2012. Testing the origin of high-energy cosmic rays. Astrophys. J. 752, 68, 19pp.

Yoon, Y.S., Ahn, H.S., Allison, P.S., et al., 2011. Cosmic-ray proton and helium spectra from the first CREAM flight. Astrophys. J. 728, 122, 8pp.

Yoon, Y.S., Anderson, T., Barrau, A., et al., 2017. Proton and helium spectra from the CREAM-III Flight. Astrophys. J. 839, 5, 8pp.